Modeling of non-isothermal CO_2 particle leaked from pressurized source: I. Behavior of single bubble

Daejun Chang*[1], Sang Heon Han[1] and Kyung-won Yang[2]

[1]*Division of Ocean Systems Engineering, Korea Advanced Institute of Science and Technology, Daejeon,Republic of Korea*
[2]*Det Norske Veritas Korea, Busan, Republic of Korea*
(Received January 9, 2012, Revised February 24, 2012, Accepted February 29, 2012)

Abstract. This study investigated the behavior of a non-isothermal CO_2 bubble formed through a leak process from a high-pressure source in a deep sea. Isenthalpic interpretation was employed to predict the state of the bubble just after the leak. Three modes of mass loss from the rising bubble were demonstrated: dissolution induced by mass transfer, condensation by heat transfer and phase separation by pressure decrease. A graphical interpretation of the last mode was provided in the pressure-enthalpy diagram. A threshold pressure (17.12 bar) was identified below which the last mode was no longer present. The second mode was as effective as the first for a bubble formed in deep water, leading to faster mass loss. To the contrary, only the first mode was active for a bubble formed in a shallow region. The third mode was insignificant for all cases.

Keywords: CO_2; bubble; depletion; dissolution; condensation; isenthalpic expansion

1. Introduction

Even in the world energy mix even in the coming decades fossil fuel is expected to take a predominant share (EIA 2009). Inevitably, the portfolio reducing greenhouse gas emissions should include CO_2 capture and storage (CCS) as a substantial component. According to the International Energy Agency (IEA) within the Organization for Economic Co-operation and Development (OECD), about one fifth of the total reduction should be treated by the CCS technology (IEA 2006). Through a techno-economic model Odenberger and Johnsson (2010) discussed the role of CCS to meet an 85% CO_2 reduction target by 2050 in EU and concluded that timely investment in CCS infrastructure should be made after 2020.

Subsea geological formations are considered to provide appropriate storage for the CCS. A plausible approach is to transport the capture CO_2 as a high-pressure gas or a supercritical fluid through pipelines into the subsea storages (Maldal and Tappel 2004, Torp and Gael 2004). An alternative is to transport CO_2 as a pressurized liquid by ship and to inject into the storage (Yoo 2010). In either case it is inevitable to install high-pressure CO_2 piping segments in the middle or the bottom of the sea.

A CO_2 leak from the high-pressure CO_2 piping segments in an oceanic area introduces critical

*Corresponding author, Professor, E-mail: djchang@kaist.edu

hazards that should deserve serious examination. A fraction of the leaked CO_2 may reach the surface and impair the safety of the personnel in the injection facilities and the CO_2 carriers because of its asphyxiating characteristics. The air with 5% CO_2 gas causes such symptoms as headache, breathing difficulty, dizziness and weakness. The concentration of 10% and 20% trigger instantaneous unconsciousness and immediate fatality (Kruse and Tekiela 1996). In addition, the atmosphere contaminated by CO_2 may not be proper for the ship engines and cause the carriers and the offshore installation to lose their prime movers. Another hazard is the low-temperature shock which may make most carbon steels brittle. The saturated vapor temperature decreases with decreasing pressure. For example, CO_2 release to the atmospheric pressure results in the vapor at -78°C. In consequence, CO_2 leak at shallow waters may pose a low-temperature risk to neighboring facilities.

The behavior of bubbles has been studied by many investigations. (Review of the studies on CO_2 droplets is available in Part II.) Kajishima *et al*. (1995) considered a gas-lift system for CO_2 release and investigated the dependence of the bubble fraction on the mass transfer coefficient. Teng *et al*. (1996) theoretically analyzed the solubility of CO_2 in the ocean and its effect on CO_2 dissolution. They predicted the shrinkage rate of CO_2 bubble, which later turned out to be in a good agreement with experimental investigations. Tsuchiya *et al*. (1997) measured the shrinkage of the bubble due to mass transfer in a pressurized liquid flowing downward and suggested a model whose predictions were in a good agreement with the experimental observation. One striking observation was that the bubble reduction rate was nearly constant irrespective of the surrounding pressure and time. (As they indicated, the deviated reduction rate in the later stage was due to nitrogen absorption.) Chen *et al*. (2009) proposed a model for an isothermal rising bubble and estimated the critical depth and the terminal time where a bubble would disappear.

In spite of the previous studies much requires some research effort. One area is the behavior of the bubbles and droplets whose is not in a thermal equilibrium with the surrounding seawater. The CO_2 leak at shallow waters results in a low-temperature bubble which is likely to absorb heat from the surroundings. This heat absorption may significantly affect the behavior of the bubble. Another area is the phase separation due to reduction in pressure. The formed bubble is close to the saturated condition. In consequence, a decrease in pressure may cause condensation of the saturated vapor. In a series of two papers, the behavior of a CO_2 particle is investigated; Part I (this paper) focuses on the bubble while Part II deals with the droplet. Even though the underlying principles are the same for the behavior of both particles, the difference in thermodynamic features between a vapor phase (the bubble) and a liquid phase (the droplet) leads to distinguished manners. One profound contrast is the direction of movement. Due to its low density, a bubble is always rising. Since the liquid CO_2 is rather compressible, its density can be higher or lower than the seawater, and the moving direction of a droplet is governed by the transient properties of the droplet just after leakage. First of all, the state of a CO_2 bubble just after leakage is interpreted assuming the enthalpy is preserved over the leakage process through which heat exchange of the bubble with the surroundings is negligible. Then, three modes of mass loss of the bubble are introduced to account for the mass transfer due to concentration gradient, heat transfer and pressure reduction. Then, follows a quantitative formulation of the three modes. In the section of Results and Discussion, representative cases are simulated numerically, and some results are presented including the evolution of the size, mass, temperature, etc. The relative magnitude of the three modes is also demonstrated.

2. Theoretical background

2.1 State immediately after leak

Consider a CO_2 leak from a pressurized source, for example, an injection riser. The high-pressure dense-phase CO_2, which may be liquid, gas or supercritical, converts to one of the following states depending on the internal condition and external pressure.

(a) Subcooled liquid
(b) Superheated vapor
(c) A mixture of saturated liquid and vapor
(d) A mixture of saturated solid and vapor
(e) Others

A leakage is an isenthalpic process. Since the line velocity through the hole is so fast that the heat exchange with the surroundings is negligible. That means, the enthalpy over the leak process is invariant. (Some authors maintained that the process would be isentropic. But, it is not reasonable to assume that the leak process accompanying an abrupt change in pressure would be reversible.) The pressure-enthalpy diagram, called the *p-h* diagram, gives an intuitive explanation of the state resulted from the leak. In Fig. 1, the initial states are denoted by S_1 to S_4, and their final states with additional alphabetical indices, A to C. State S_1 is a subcooled liquid while the others are supercritical with their pressure and temperature greater than the critical pressure and temperature, respectively. For a given initial state the pressure just after the leak, P_0, which is determined by the water depth, governs the state of the leaked fluid. Consider State S_1. When P_0 is greater than the saturated vapor pressure, the leaked fluid is still a subcooled liquid at State $S_{1,A}$. If P_0 is lower than the saturated pressure and greater than the triple point pressure, the leaked fluid at $S_{1,B}$ is a mixture of vapor and liquid. For P_0 less than the triple point pressure, a mixture of solid and vapor is observed. The same reasoning is applicable to the other initial states with some features modified. Expansion with the initial state S_2, which is a supercritical phase, results in the similar observations to that with State S_1. Expansion with the initial state S_3, however, leads to a slightly different

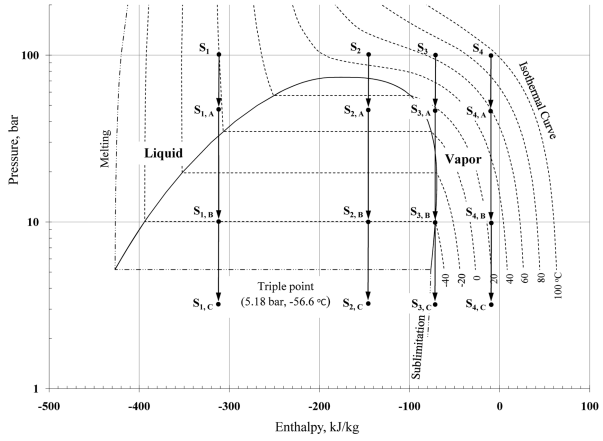

Fig. 1. Initial states and their final states with surrounding pressure

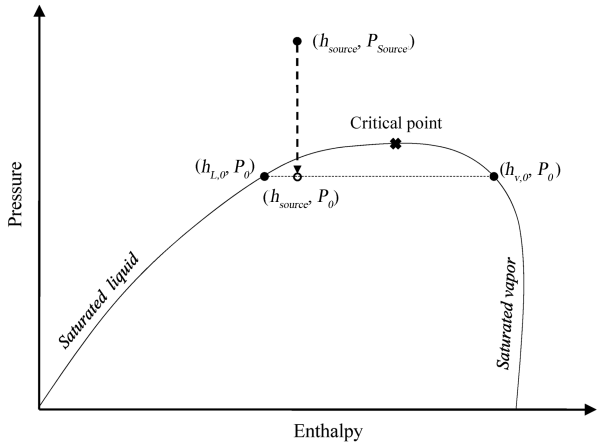

Fig. 2. State immediately after leak

consequence that State $S_{3,C}$ is a vapor phase. When the enthalpy is sufficiently high (for example, State S_4), expansion of the fluid only results in a vapor phase, regardless of P_0.

The fraction of the vapor and liquid after leak can be estimated by the level rule (King 1980), which is just a statement of the enthalpy conservation over the leak process in spite of phase separation. Consider Fig. 2 where the fluid at pressure P_{Source} is released through a hole to the surrounding water at pressure P_0. Since the enthalpy is preserved, the transition is from (h_{Source}, P_{Source}) to (h_{Source}, P_0). When the resulting point is within the envelop of the saturated liquid-vapor curves, the resulting fluid is a mixture of a liquid phase at Point ($h_{L,0}$, P_0) and Point ($h_{V,0}$, P_0). The lever rule states that the mass fraction of the liquid phase to the liquid one is given by the relative distance from the saturated curves.

$$\Gamma_{Leak,L} = \frac{h_{V,0} - h_{Source}}{h_{V,0} - h_{L,0}} = \frac{h_{V,0} - h_{Source}}{h_{LV}(P_0)} \tag{1}$$

Here, $h_{LV}(P_i)$ is the heat of vaporization at pressure of P_i It should be noted that the bubble may be in a significantly low temperature. Consider the isothermal curves in Fig. 1. For a given enthalpy, the temperature is increasing with pressure. It implies that the decrease in pressure through leak process leads to a drop in temperature.

2.2 Three modes of mass loss

When the bubble is placed in the middle of water, it loses its mass to the surrounding water. The mass loss from the bubble is categorized into three modes based on the driving potentials: concentration, temperature and pressure differences.

Mode V.1: Dissolution induced by mass transfer

Mode V.2: Condensation induced by heat transfer

Mode V.3: Phase separation induced by pressure decrease

The magnitude of the modes depends on the circumstance. Mode V.1 is universal for all cases since the bubble is always in a higher concentration than the surrounding water. As the concentration of CO_2 in the water increases, Mode V.1 becomes weak. Mode V.2 is valid only if

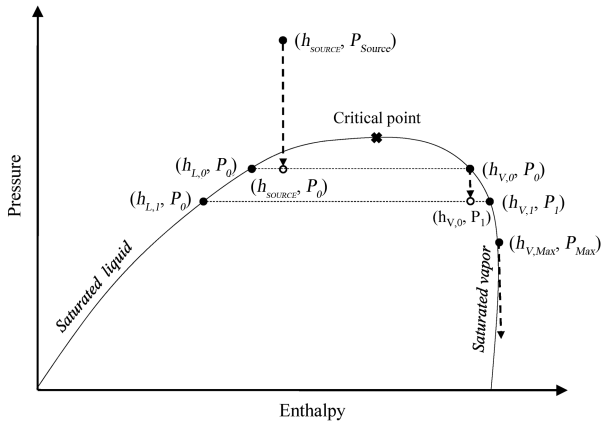

Fig. 3. New vapor-liquid equilibrium caused by change in pressure

there is a temperature gradient. As explained earlier, the leaked CO_2 has a significant temperature difference from the surrounding water. Consequently, Mode V.2 does not vanish until the bubble is in thermal equilibrium with the surrounding water. Mode V.3 is a kind of adiabatic condensation resulted from the isenthalpic expansion to establish a new vapor-liquid equilibrium due to the decrease in the surrounding pressure as the bubble moves upward. Consider Fig. 3 where a pressure-induced equilibrium is presented with the state developed by the leak process. Intrinsically, they are governed by the same principle that the decrease in pressure should cause the phase separation to occur if the resulting condition is within the envelop of the saturated liquid-vapor curve. The pressure is decreased from P_0 to P_1 due to the rising bubble motion. Accordingly, the enthalpy is changed from State ($h_{V,0}$, P_0) to State ($h_{V,0}$, P_1) with the enthalpy preserved. Since the latter point is a mixture of liquid and vapor, it separates into a liquid phase at State ($h_{L,1}$, P_1) and State ($h_{V,1}$, P_1). Analogous to Eq. (1), the mass fraction of the liquid phase is given by the equation.

$$\Gamma_L(0,1) = \frac{h_{V,1} - h_{V,0}}{h_{V,1} - h_{L,1}} = \frac{h_{V,1} - h_{V,0}}{h_{LV}(P_1)} \tag{2}$$

In reality, the bubble movement is far slower than the phase separation, and the phase separation process occurs continuously rather than the discrete way which was taken for the convenience of explanation. That is, the bubble follows the saturated vapor curve, accompanying the liquid condensation. Since the enthalpy of the saturated vapor is convex to the right-hand side, the condensation due to the expansion no longer exists for the region where the pressure is less than P_{Max}, which is equal to 17.12 bar, as shown in Fig. 3. Starting from the critical point, the enthalpy of the saturated vapor with respect to pressure is increasing to $h_{V,Max}$ at P_{Max}, and then decreasing from the maximum. In the region where the pressure is less than P_{Max}, expansion does not lead the vapor in the bubble to fall into the saturated vapor-liquid envelop, implying that no condensation occurs during the process.

3. Formulation

3.1 Assumptions

Consider Fig. 4 where a bubble is placed at the depth H(t). Its temperature is different from that of the surrounding water, and so are the viscosity and the density. Due to the difference in density, it rises with the velocity, $u_V(t)$ Let $\Delta m_{V,M}$(t), $\Delta m_{V,T}$(t), and $\Delta m_{V,P}$(t) denote the mass loss of Modes V.1, V.2, and V.3, respectively. Note that the mass losses are defined positive. Based on the theoretical background in Section 2, the following assumptions are employed.

A1. A bubble is formed from a liquid jet via isenthalpic expansion and initially at a saturated vapor state when the surrounding pressure is less than the saturated pressure.

A2. The bubble is placed in an infinite large quiescent flow field.

A3. The shape of bubble is spherical for mass transfer estimation. For estimation of the terminal velocity, deformation of the bubble is considered.

A4. The bubble is free of ice or hydrate formation.

A5. The mass loss due to Mode V.1 is independent of Modes V.2 and V.3.

A6. When the pressure is less than P_{Max}, the phase separation does not occur, and the mass loss due to Modes V.2 and V.3 is not effective.

A7. When the heat egress is positive, and the pressure is greater than P_{Max}, Mode V.2 results in condensation.

A8. When the heat egress is negative, Mode V.2 leads to an increase in the temperature of the bubble.

A9.Once the condensed CO_2 is formed, it separates from the bubble and immediately disperses into the surrounding medium.

3.2 Mode V.1 dissolution induced by mass transfer gradient

The difference in CO_2 concentration between the bubble and the surrounding seawater causes a mass transfer from the bubble. Assuming the seawater interfaced with the bubble is saturated with CO_2, the mass flux is given by the equation.

$$J_{V,M}(t) = Wh_{V,M}(c^{\#} - c^{\infty}) \tag{3}$$

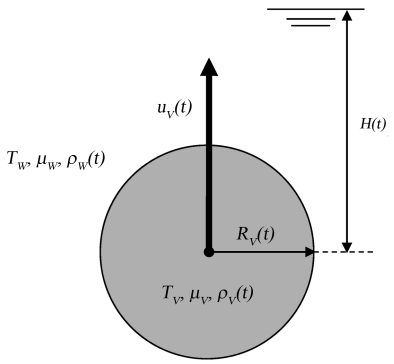

Fig. 4. Definition of state variables

Here, $c^{\#}$ and c^{∞} are the concentrations of the dissolved CO_2 on the interface and in the far field. And, W is the molecular weight of CO_2. The dissolved mass due to the concentration gradient, $m_{V,M}(t)$, for time interval Δt is given by multiplying the mass flux by the surface area of the bubble, A(t).

$$\Delta m_{v,M}(t) = A(t) J_{V,M}(t) \Delta t \tag{4}$$

The mass conservation relates the mass reduction with the mass transfer rate.

$$\frac{d}{dt}(m_V) = -A(t)\, J_{V,M}(t) \tag{5}$$

For a spherical bubble, Eq. (5) becomes the following expression.

$$\frac{d}{dt}\left(\frac{4}{3}\pi R_V^3 \rho_V\right) = -4\pi R_V^2\, W h_{V,M}(c^{\#} - c^{\infty}) \tag{6}$$

Under constant pressure circumstance, Eq. (6) reduces to the expression.

$$\frac{dR_V}{dt} = -\frac{W h_{V,M}(c^{\#} - c^{\infty})}{\rho_V} \tag{7}$$

Under normal circumstance ρ_V is linearly proportional to $c^{\#}$, and c^{∞} is effectively zero. Unless the mass transfer $h_{L,M}$ is a strong function of the radius; the radius reduction rate is nearly invariant irrespective of the surrounding pressure and the bubble size. Based on their theoretical and experimental study, Tsuchiya *et al*. (1997) showed that the radius of bubble is a linear function of time.

$$R_V(t) = R_V(0) - \Phi_{V,M}\, t \tag{8}$$

From Fig. 8 of their study, the reduction rate for the NaCl solution with 3.0 wt% is taken.

$$\Phi_{V,M} = 2.0 \times 10^{-4} \text{ m/s} \tag{9}$$

Rearranging Eq. (3) gives an expression for the mass flux.

$$J_{V,M}(t) = W h_{V,M}(c^{\#} - c^{\infty}) = \rho_V(t) \Phi_{V,M} \tag{10}$$

The dissolved mass due to the concentration gradient is given by the equation.

$$\Delta m_{V,M}(t) = A(t) J_{V,M}(t) \Delta t = A(t) \rho_V(t) \Phi_{V,M} \Delta t \tag{11}$$

3.3 Mode V.2 condensation induced by heat transfer

The significant temperature difference between the bubble and the surrounding seawater cause

heat flux into the bubble.

$$J_{V,T}(t) = h_{V,T}(t)(T_V - T_W^{\infty}) \tag{12}$$

Here, T_W^{∞} is the temperature of the surrounding water outside the boundary layer. The total heat ingress rate over the surface is given by multiplying the heat flux with the surface area. The evaporation mass due to the heat ingress, $\Delta m_{V,T}(t)$, for time interval Δt is given by dividing the heat ingress by heat of vaporization.

$$\Delta m_{V,T}(t) = \frac{A(t)J_{V,T}(t)}{h_{LV}(t)}\Delta t \tag{13}$$

The heat transfer coefficient is estimated by the correlation (Clift *et al*. 1978, Chen *et al*. 2009).

$$Nu = 1 + (1 + Pe)^{1/3} \tag{14}$$

Here, the dimensionless numbers are defined as follows.

$$Nu = \frac{2R_V h_{V,T}}{k_W} \tag{15}$$

$$Pe = RePr \tag{16}$$

$$Pr = \frac{\mu_W C_{P,W}}{k_W} \tag{17}$$

$$Re = \frac{2R_V \rho_W u_V}{\mu_W} \tag{18}$$

3.4 Mode V.3 phase separation induced by pressure decrease

The pressure decrease caused by a movement with velocity $u_V(t)$ for time interval Δt is given by the equation.

$$\Delta P_{V,P}(t) = g\rho_W u_V(t)\Delta t \tag{19}$$

Consider the isenthalpic transition from Point ($h_{V,n}$, P_n) by the pressure difference to Point ($h_{V,n}$, P_{n+1}) as shown in Fig. 5. As explained in Eq. (2), the mass fraction of the condensed liquid is given by the lever rule.

$$\Gamma_L(n, n+1) = \frac{h_{V,n+1} - h_{V,n}}{h_{V,n+1} - h_{L,n+1}} = \frac{h_{V,n+1} - h_{V,n}}{h_{LV}(P_{n+1})} \tag{20}$$

The condensation mass loss due to the pressure change, $\Delta m_{V,P}(t)$, for time interval Δt is given by multiplying the bubble mass by the vapor fraction ratio.

$$\Delta m_{V,P}(t) = m_V(t)\Gamma_L(n, n+1) \tag{21}$$

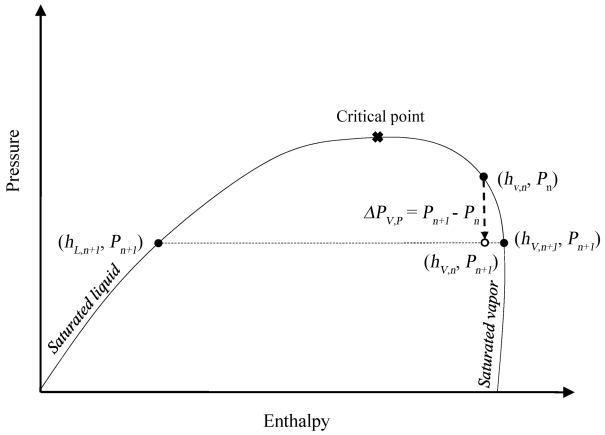

Fig. 5. Evolution of saturated state due to pressure change caused by bubble's rising motion

The mass change due to Mode V.3 is proportional to the volume while those due to Modes V.1 and V.2 increases with the surface area.

3.5 Terminal velocity

The terminal velocity of a bubble is expressed by the expression (Clift *et al*. 1978, Chen *et al*. 2009).

$$u_V = \frac{\mu_W}{2\rho_W R_V} Mo^{-0.149}(J - 0.857) \tag{22}$$

Here, the Morton number is defined as follows.

$$Mo = \frac{g\mu_V^4(\rho_W - \rho_V)}{\rho_W^2 \sigma^3} \tag{23}$$

The dimensionless parameter J is a function of the Eötvös number (Eo) as well as the Morton number and the viscosity ratio.

$$J = \begin{cases} 0.94\Theta^{0.757} & 2 < \Theta \le 59.3 \\ 3.42\Theta^{0.441} & \Theta > 59.3 \end{cases} \tag{24}$$

$$\Theta = \frac{4}{3} Eo\, Mo^{-0.149} \left(\frac{\mu_V}{\mu_W} \right)^{-0.14} \tag{25}$$

$$\mathrm{Eo} = \frac{4g(\rho_W - \rho_V)R_V^2}{\sigma} \tag{26}$$

Unlike the Stokes velocity, the terminal velocity of a bubble is not proportional to the particle size. Instead, the terminal velocity becomes rather constant with the bubble size (See Fig. 7.3 of Clift *et al*. 2009).

4. Results and discussion

4.1 Bubble size distribution

For numerical simulation, this study considers a saturated bubble formed from a leak at the depth of 50 m, 200 m, and 500 m. The bubble radius is assumed to be 0.025 m, which is the possible maximum size for an air bubble in water. (See Eqs. (12)-(46) and Table 12.3 of Clift *et al*. 2009). The surrounding seawater is assumed to have constant physical properties, as shown in Table 1. It is assumed that the sea water temperature should be constant at 10°C with salinity of 30 g/kg. Other properties are referred to the study done by Sharqawy *et al*. (2011). The CO_2 bubble may experience a considerable change in pressure and temperature, as discussed previously. A commercial database, called CO_2Tab^{TM}, is used for the physical properties of CO_2.

The evolution of the bubble size is shown in Fig. 6. The bubbled formed at H(0) = 200 m and 50 m exists up to 100 seconds. Considering the bubble size and the radius reduction rate in Eq. (9), the time duration indicates that only Mode V.1 is effective. To the contrary, the bubble generated at H(0) = 500 m disappears around 60 seconds, implying that one or both of the other two modes are

Table 1 Properties of seawater

Parameter	Notation	Value		Reference
Temperature	T_W	10	°C	
Salinity		30	g/kg	
Viscosity	μ_W	0.001382	kg/m/s	Sharqawy *et al*. 2011
Density	ρ_W	1023	kg/m^3	Sharqawy *et al*. 2011
Specific heat	$C_{p,W}$	4022	J/kg/°C	Sharqawy *et al*. 2011
Thermal conductivity	k_W	0.587	W/m/°C	Sharqawy *et al*. 2011
Prandtl number	Pr	9.47		Sharqawy *et al*. 2011
Surface tension	σ	0.03	N/m	Chen *et al*. 2009

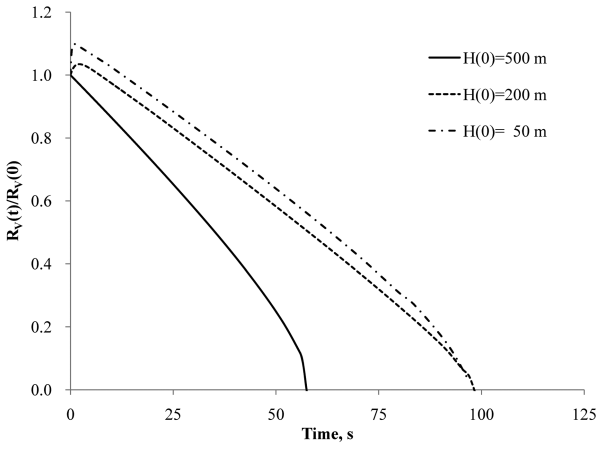

Fig. 6. Bubble radius with time

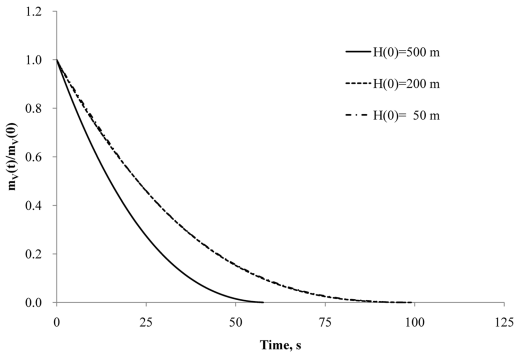

Fig. 7. Instant mass with time

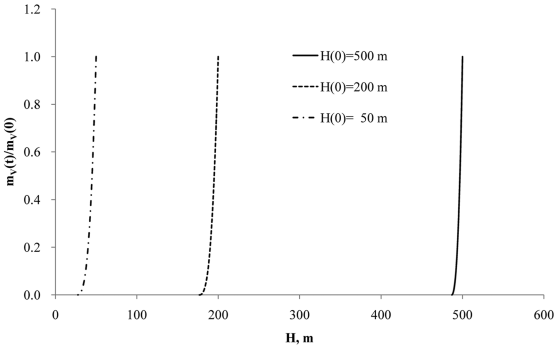

Fig. 8. Instant mass with depth

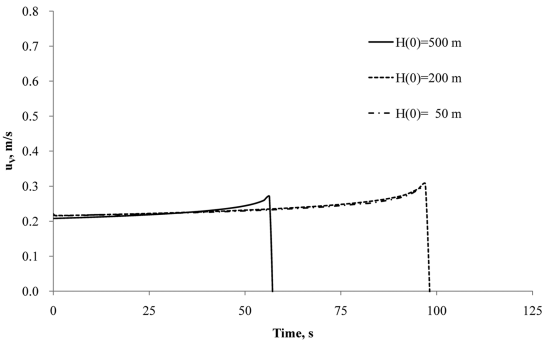

Fig. 9. Bubble velocity with time

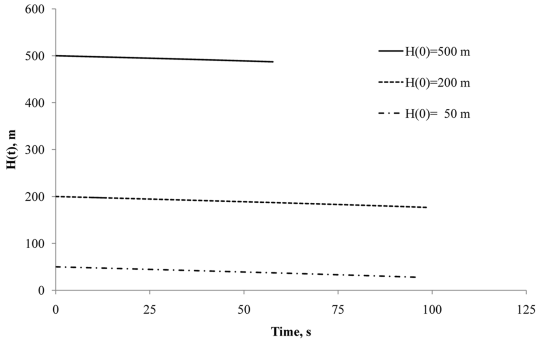

Fig. 10. Bubble position with time

effective in this case. This implication will be clarified later.

The mass change shows a little different feature. Fig. 7 shows the ratio of the instant mass to the initial mass with time. As in Fig. 7, the mass loss rate is far greater for the bubble formed at H(0) = 500 m than for the others. The curves for H(0) = 200 m and 50 m overlap each other, implying that the active modes for the mass loss are identical for them. Fig. 8 is another presentation of the ratio in terms of depth. For all the cases, the bubbles cease to exist after traveling about 50 meters. This observation is important from the view point of safety. In these cases, all the bubbles lose their mass into the seawater, resulting in negligible impact on the safety of the crew in the ship or the offshore installation.

The rising velocity of the bubbles is nearly constant in spite of the time as well as the leakage depth, as shown in Fig. 9. The initial speed is around 0.2 m/s for all the three bubbles. As they rise with time, their size changes significantly as shown in Fig. 6. Nevertheless, their speed remains relatively constant except when the bubble is significantly small. That is because the terminal velocity of a bubble is nearly independent of its size, as well explained in (Clift *et al*. 1978) (See Fig. 7.3 of the book). The constant rising velocity causes the depth of the bubbles to decrease linearly with time as shown in Fig. 10. Note that the curves are practically straight lines with constant slopes, and the slopes, equivalently the rising velocities, are virtually equal to the others.

The temperature of the bubbles is shown in Fig. 11. The temperature of the bubbles generated at H(0) = 200 m and 50 m approaches the seawater temperature within 5 seconds. To the contrary, the bubble formed at H(0) = 500 m preserves its higher temperature for a while. This contrasting

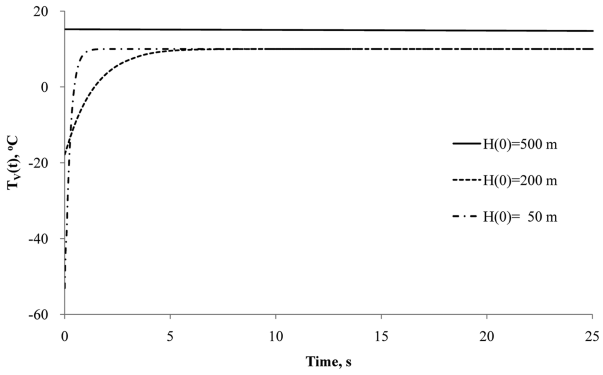

Fig. 11. Bubble temperature with time

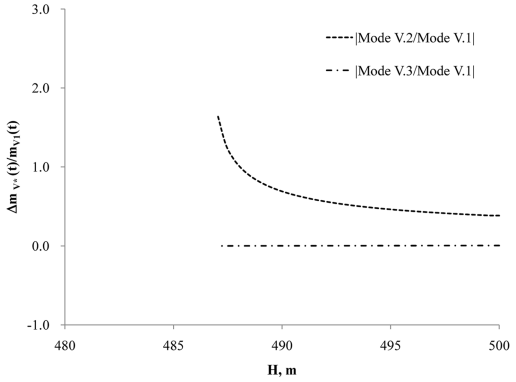

Fig. 12 Magnitude of mass loss modes normalized by Mode V.1 for leak at 500 m

behavior is in accordance with the explanation of Section 2. THEORETICAL BACKGROUND. When the bubble pressure is far greater than P_{max}, the bubble may undergoes phase separation following the saturated vapor curve in Fig. 3. In this case, the bubble temperature is given by the surrounding pressure. When the bubble pressure is around P_{max} or smaller, the bubble undergoes expansion free from liquid-vapor equilibrium, pursuing the surrounding temperature. In this case, the bubble temperature is given by the surrounding temperature, not by the surrounding pressure.

Fig. 12 shows the normalized magnitude of the mass loss modes for the bubble formed at H(0) = 500 m. Compared with Mode V.1 which is constant as designated by Eqs. (9) and (11), Mode V.3 is negligible and Mode V.2 is as effective as Mode V.1. The temperature of the bubble higher than the surroundings causes the heat to transfer from the bubble, resulting in condensation of part of the vapor in the bubble. That is why the mass loss rate for the bubble in Fig. 7 nearly doubles that of the others.

Fig. 13 shows the normalized magnitude of the mass loss modes for the bubble generated at H(0) = 200 m. Just after its formation, the bubble temperature is even lower than the seawater as shown in Fig. 11, and Mode V.2 is considerable due to the significant temperature difference. Traveling about 2 meters, the bubble temperature is close to the surroundings, and the Mode V.2 becomes insignificant. Then, only Mode V.1 is effective. The magnitude of Mode V.2 is the same for the bubble formed at H(0) = 50 m. A significant impact of Mode V.2 is short-lived. Note that Mode V.3 is not active in this case since the surrounding pressure is less than P_{max}.

5. Conclusions

The three modes of mass loss from a non-isothermal bubble were demonstrated. Mode V.1 Dissolution was induced by mass transfer while Mode V.2 Condensation and Mode V.3 Phase separation were caused by heat transfer and pressure decrease, respectively. A graphical interpretation of the last mode was provided in a pressure-enthalpy diagram. There was a threshold pressure of 17.12 bar below which Mode V.3 was absent. For a bubble formed in a deep region where the hydrostatic pressure far greater than the threshold pressure, Mode V.2 was as effective as Mode V.1. To the contrary, for a shallow leak, the bubble temperature was significantly lower than the surrounding seawater, and Mode 2 was dominant just for a short period. In overall, Mode V.1

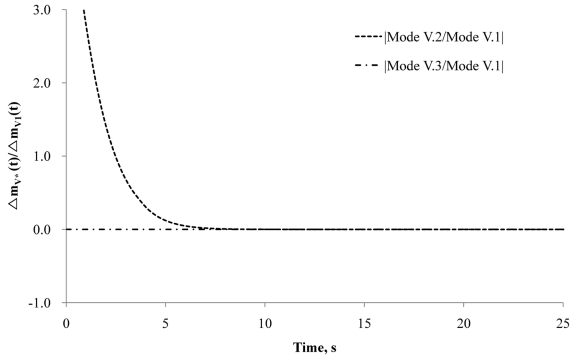

Fig. 13 Mass loss modes with depth for leak at 200 m

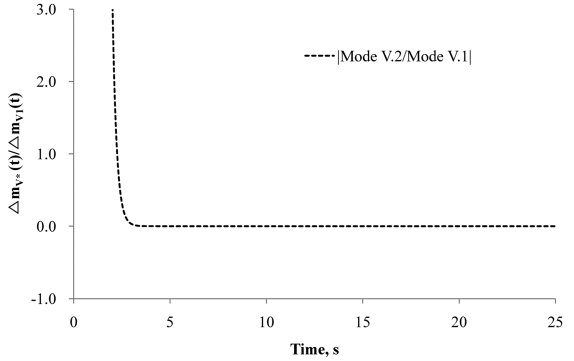

Fig. 14 Mass loss modes with depth for leak at 50 m

was the only mode effective for the shallow-water bubbles.

Some areas require further research effort. One is the effect of the bubble deformation. Under the condition identified in this study, the bubble shape seems to be ellipsoidal or spherical-cap. Even for the shape far from a sphere, the terminal velocity is well approximated by Eq. (22), and Mode V.3 is independent of the shape. Mode V.2 and Mode V.3 may be affected by the deformation. Another area is the behavior of the aggregated bubbles. When the leak amount is considerable, a large number of bubbles would be formed and rise in group. In that case, the prediction based on a single bubble may be limited. Analysis of this phenomenon is absolutely important to the risk to the personnel risk.

Acknowledgements

This research was supported by a grant from the LNG Plant R&D Center funded by the Ministry of Land, Transportation and Maritime Affairs (MLTM) of the Korean government.

References

Chen, B., Nishio, M., Song, Y. and Akai, M. (2009), "The fate of CO2 bubble leaked from seabed", *Energ.Procedia*, **1**(1), 4969-4976.

Clift, R., Grace, J.R. and Weber, M.E. (1978), *Bubbles, drops, and particles*, Dover Publication Inc., New York.

International Energy Agency (IEA) (2006), Energy Technology Perspectives 2006: Scenarios & Strategies to 2050.

Energy Information Administration (EIA) (2009), *International Energy Outlook 2009*, U.S. Energy Information Administration, Report No. DOE/EIA-0484.

Kajishima, T., Saito, T., Nagaosa, R. and Hatano, H. (1995), "A gas-lift system for CO2 release into shallow seawater", *Energ. Convers. Manage*., **36**(6-9), 467-470.

King, C.J. (1980), *Separation Processes,* 2nd Ed., McGraw-Hill book company, New York.

Kruse, H. and Tekiela, M. (1996), "Calculating the consequences of a CO2-pipeline rupture", *Energ. Convers. Manage*., **37**(6-8), 1013-1018.

Maldal., T. and Tappel, I.M. (2004), "CO2 underground storage for Snøhvit gas field development", *Energy*, **29**(9-10), 1403-1411.

Odenberger, M. and Johnsson, F. (2010), "Pathways for the European electricity supply system to 2050-The role

of CCS to meet stringent CO2 reduction target", *Int. J. Greenh. Gas Con*., **4**(2), 327-340.
Sharqawy, M.H., Lienhard J.H. and Zubari, S.M. (2011), "On exergy calculations of seawater with applications in desalination system", *Int. J. Therm. Sci*., **50**(2), 187-196.
Teng, H., Masutani, S.M., Kinoshita, C.M. and Nihous, G.C. (1996), "Solubility of CO2 in the ocean and its effect on CO2 dissolution", *Energ. Convers. Manage*., **37**(6-8), 1029-1038.
Torp, T.A. and Gale, J. (2004), "Demonstrating storage of CO2 in geological reservoirs: The Sleipner and SACS projects", *Energy*, **29**(9-10), 1361-1369.
Tsuchiya, K., Mikasa, H. and Saito, T. (1997), "Absorption dynamics of CO2 bubbles in a pressurized liquid flowing downward and its simulation in seawater", *Chem. Eng. Sci*., **52**(21-22), 4119-4126.
Yoo, B. (2010), "Achieving viability: deliver an integrated shipping solution for CCS using CO2 shipping", *Proceedings of the CO2 Shipping conference 2010*, London, May.

Nomenclature

Alphabets

A	Surface area of the bubble, m^2
B	Reduction rate of the bubble radius, m/s
C	Heat capacity, $J(/(\mathrm{kg} \cdot {}^{\circ}\mathrm{C})$
$c^{\#}$	CO_2 concentration on the interface between the bubble and the water, mol/m^3
c^{∞}	CO_2 concentration in the far field, mol/m^3
u_V	Terminal velocity of a CO_2 bubble, m/s
H	Depth, m
$h_{V,M}$	Mass transfer coefficient, m/s
$h_{V,T}$	Heat transfer coefficient, $J(/(\mathrm{m} \cdot {}^{2}s \cdot {}^{\circ}\mathrm{C})$
h_{Source}	Enthalpy of high-pressure source, J/kg
h_{LV}	Heat of vaporization, J/kg
$h_{L,i}$	Enthalpy of liquid phase at state i, J/kg
$h_{V,i}$	Enthalpy of vapor phase at state i, J/kg
g	Gravitational acceleration, m/s^2
$J_{V,M}$	Mass flux, $kg/(m^2 \cdot s)$
$J_{V,T}$	Heat flux, $J/(m^2 \cdot s)$
k	Thermal conductivity, $J/(m \cdot s)$
m	Mass, kg
$\Delta m_{V,M}$	Mass loss through Mode V.1 Dissolution induced by mass transfer, kg
$\Delta m_{V,T}$	Mass loss through Mode V.2 Condensation induced by heat transfer, kg
$\Delta m_{V,P}$	Mass loss through Mode V.3 Phase separation induced by pressure decrease, kg
P	Pressure, N/m^2
R	Radius of the bubble, m
S	State
T	Temperature, $^{\circ}C$
W	Molecular weight of CO_2, kg/mol

Greeks

$\Gamma_{Lesk,L}$	Liquid mass fraction just after leak
$\Gamma_{L(i,j)}$	Liquid mass fraction over transition from State i to State j

ρ	Density, kg/m^3
σ	Surface tension, N/m

Subscripts

V	CO_2 vapor phase
W	Water phase